TISSUE ENGINEERING: Part A
Volume 24, Numbers 5 and 6, 2018

DOI: 10.1089/ten.tea.2016.0400

termis
Tissue Engineering
& Regenerative Medicine
International Society

ORIGINAL ARTICLE

Derivation of Cortical Spheroids from Human Induced Pluripotent Stem Cells in a Suspension Bioreactor

Yuanwei Yan, PhD,* Liqing Song, MS, Jason Madinya, BS,† Teng Ma, PhD, and Yan Li, PhD

Human induced pluripotent stem cells (hiPSCs) emerge as a promising source to construct human brain-like tissues, spheroids, or organoids *in vitro* for disease modeling and drug screening. A suspension bioreactor can be used to generate large size of brain organoids from hiPSCs through enhanced diffusion, but the influence of a dynamic bioreactor culture environment on neural tissue patterning from hiPSCs has not been well understood. The objective of this study is to assess the influence of a suspension bioreactor culture on cortical spheroid (*i.e.*, forebrain-like aggregates) formation from hiPSCs. Single undifferentiated hiPSK3 cells or preformed embryoid bodies were inoculated into the bioreactor. Aggregate size distribution, neural marker expression (e.g., Nestin, PAX6, β-tubulin III, and MAP-2), and cortical tissue patterning markers (e.g., TBR1, BRN2, SATB2, and vGlut1) were evaluated with static control. Bioreactor culture was found to promote the expression of TBR1, a deep cortical layer VI marker, and temporally affect SATB2, a superficial cortical layer II–IV marker that appears later according to inside-out cortical tissue development. Prolonged culture after 70 days showed layer-specific cortical structure in the spheroids. Differential expression of matrix metalloproteinase-2 and −3 was also observed for bioreactor and static culture. The altered expression of cortical markers by a suspension bioreactor indicates the importance of culture environment on cortical tissue development from hiPSCs.

Keywords: human pluripotent stem cells, neural differentiation, cortical spheroids, suspension culture, bioreactor

Introduction

Recapitulating neural development and pathology in a 3D human brain tissue model is critical for studying disease progression and screening drugs for the treatment of neurological diseases such as Alzheimer's disease.[1–4] Human cerebral cortex is different from that of the rodent due to the significantly increased size, complexity, and the increase in layer diversity and neuronal cell types.[5] Recently, *in vitro* 3-D neural cell cultures have been investigated to mimic forebrain cortical tissue.[1,6] However, these 3D models were established using adult human neural stem cells and restricted access to human brain tissues limits the distribution of such models. Human induced pluripotent stem cells (hiPSCs) have great potential to generate allogeneic or patient-specific cortical cells, tissues, and ''mini-brains'' (also known as brain spheroids/organoids) that are physiologically relevant to model neurological diseases.[7–14] While some disease progression (e.g., amyloid-β plaques) may take years, *in vitro* cortical organoids derived from hiPSCs can be used to probe early stages of disease onset and identify pharmacological therapeutics.[13] For example, amyloid β (Aβ)-secreting neurons derived from hiPSCs have been used to screen anti-Aβ drugs and evaluate Aβ-induced toxicity.[9,15,16] Compared to 2D culture models, 3D cortical neural culture models were shown to promote neuronal maturation and better recapitulation of neurological disease pathology.[1,17] Therefore, hiPSC-derived cortical organoids provide valuable forebrain-like tissue models with human genetic background for neurological disease modeling, drug screening, and studying virus infection (e.g., Zika virus).[18]

A dynamic spinner bioreactor culture enhances diffusion in neural progenitor cell (NPC) spheres derived from hiPSCs and allows further growth and maturation of large size aggregates (up to 4 mm in diameter).[10,18] While the ultimate

Department of Chemical and Biomedical Engineering, FAMU-FSU College of Engineering, Florida State University, Tallahassee, Florida.

The preliminary results of this study were presented at the 2016 annual meeting of American Institute of Chemical Engineers (AIChE), November 13–18, 2016, San Francisco, California.

Current affiliation: Waisman Center, University of Wisconsin-Madison, Madison, Wisconsin.
†*Current affiliation*: Department of Chemical and Biomolecular Engineering, University of Illinois at Urbana—Champaign, Urbana, Illinois.

solution to generate large size of forebrain tissues needs the vascularization of the constructs,[4,19] bioreactor culture provides an immediate and simple approach for the human PSC (hPSC)-derived aggregate development into mini-tissues through enhanced diffusion.[20] The suspension-based stirred bioreactor is simple, scalable, and has the potential to generate a large quantity of cortical organoids for downstream applications in drug screening and disease modeling. Generation of stem cell spheroids or organoids in a suspension bioreactor has been demonstrated for mesenchymal stem cells, hPSC-derived cardiac cells, and hPSC-derived NPCs.[20–24] The size of stem cell aggregates can be regulated by agitation speed/shear stress, which indirectly affects the diffusion of biomolecules.[25–27] Collectively, the simple setup of suspension bioreactor allows us to delineate the complex biological problems involved in cortical tissue development from hPSCs. However, the influence of suspension bioreactors on brain tissue structure has not been well explored.

The objective of this study is to investigate the effect of dynamic bioreactor culture on the formation of cortical spheroids from hiPSCs. Current systems have derived cortical cells or spheroids from hPSCs in static cultures.[2,28] How dynamic bioreactor culture impacts the development of cortical tissues from hPSCs remains unclear. In addition, current methods to derive cortical organoids from hPSCs involve long-term culture (up to 140 days). It would be advantageous if the developmental time is shortened by modulating the culture system. In this study, it is hypothesized that cortical tissue development from hiPSCs may be accelerated by the dynamic culture due to enhanced diffusion of patterning factors. So this study compared the aggregate formation from hiPSCs, neural patterning marker expression, and the expression of cortical layer-specific genes in a spinner bioreactor and a static culture. To evaluate the temporal effect of bioreactor culture, the inoculation with single hiPSC suspension and preformed embryoid bodies (EBs) was investigated. The outcome of this study should provide the knowledge on cortical tissue development from hPSCs and a transformative platform to generate cortical spheroids or organoids for disease modeling, drug screening, and possibly cell therapy.

Materials and Methods

Undifferentiated human iPSC culture

Human iPSK3 cells were derived from human foreskin fibroblasts transfected with plasmid DNA encoding reprogramming factors OCT4, NANOG, SOX2, and LIN28 (kindly provided by Dr. Stephen Duncan, Medical College of Wisconsin, and Dr. David Gilbert, Department of Biological Sciences of Florida State University).[29,30] Human iPSK3 cells were maintained in mTeSR serum-free medium (StemCell Technologies, Inc., Vancouver, Canada) on six-well plates coated with growth factor-reduced Geltrex (Life Technologies). The cells were passaged by Accutase dissociation every 5–6 days and seeded at 1×10^6 cells per well of six-well plate in the presence of 10 μM Y27632 (Sigma) for the first 24 h.[31]

Neural differentiation and cortical spheroid formation from hiPSCs in static culture

For neural differentiation in static culture, human iPSK3 cells were seeded into ultra-low attachment 24-well plates (Corning Incorporated, Corning, NY) at $4.0–4.5 \times 10^5$ cells per well in 1 mL of differentiation medium composed of Dulbecco's Modified Eagle Medium/Nutrient Mixture F-12 (DMEM/F-12) plus 2% B27 serum-free supplement (Life Technologies).[32] Y27632 (10 μM) was added during the seeding and removed after 24 h. On day 1, the cells formed EBs and were treated with no growth factor or with dual SMAD signaling inhibitors: 10 μM SB431542 (Sigma) and 100 nM LDN193189 (Sigma), hereafter referred to as LDN/SB. After 7 days, the cells were treated with cyclopamine (1 μM) and fibroblast growth factor-2 (10 ng/mL) until day 14. The suspension cultures were maintained for 7 days in short-term study or for 21–71 days in long-term study. For immunocytochemistry characterizations, the aggregates were replated onto Geltrex-coated surface for 5–7 days.

Preparation of spinner bioreactors

A 50 mL glass spinner bioreactor (#356875; Wheaton) was used for studying NPC differentiation and neural tissue patterning from hiPSCs. Before the inoculation, the vessel was immersed with 2 mL Sigmacote (#SL2; Sigma) overnight to avoid cell attachment on the glass surface. Then, the vessel was dried at room temperature. The spinner bioreactor was autoclaved at 121°C for 20 min before using. Wheaton Micro-Stir platform (#W900701-A; Wheaton) was used for bioreactor culture. The Micro-Stir platform allows for the control of agitation speed and the pattern (e.g., intermittent agitation with different cycles).[33] The Micro-Stir platform was put into a 37°C, 5% CO_2 incubator before setting up bioreactor culture (Fig. 1A).

Neural induction and cortical spheroid formation from hiPSCs in bioreactor culture

The bioreactor was inoculated with day 0 undifferentiated hiPSK3 single cell suspension in the presence of Y27632 or day 8 EBs, in parallel to static control. For undifferentiated cells, the seeding density was $4.0–4.5 \times 10^5$ cells/mL. Alternatively, the EBs formed with the equivalent cell density to static culture were put in the bioreactor. The working volume of the bioreactor was 15 mL. After single-cell inoculation, the bioreactor was agitated at an intermittent mode (15-min on/15-min off cycle for 12 h) at 80 rpm. After that, a constant agitation (100 rpm) was maintained until the harvest time (day 7–67 in bioreactor). For EB inoculation, the bioreactor was agitated at a constant speed (100 rpm) until the harvest time. Complete medium change was performed every 3–4 days. During the culture time, samples were taken to monitor aggregate size distribution, glucose consumption, and lactate production. The cell numbers were determined at the harvest time by counting a 2 mL aggregate sample. The harvested aggregates were either replated to Geltrex-coated surface for another 4–7 days for immunocytochemistry, flow cytometry, or reverse transcription–polymerase chain reaction (RT-PCR) analysis, or kept in low-attachment plates (up to a total of 71-day culture) for confocal microcopy analysis.

Aggregate size distribution

The images of aggregates (both the bioreactor and static culture in the side-by-side comparison of the same experiment) were captured over the culture time by phase-contrast

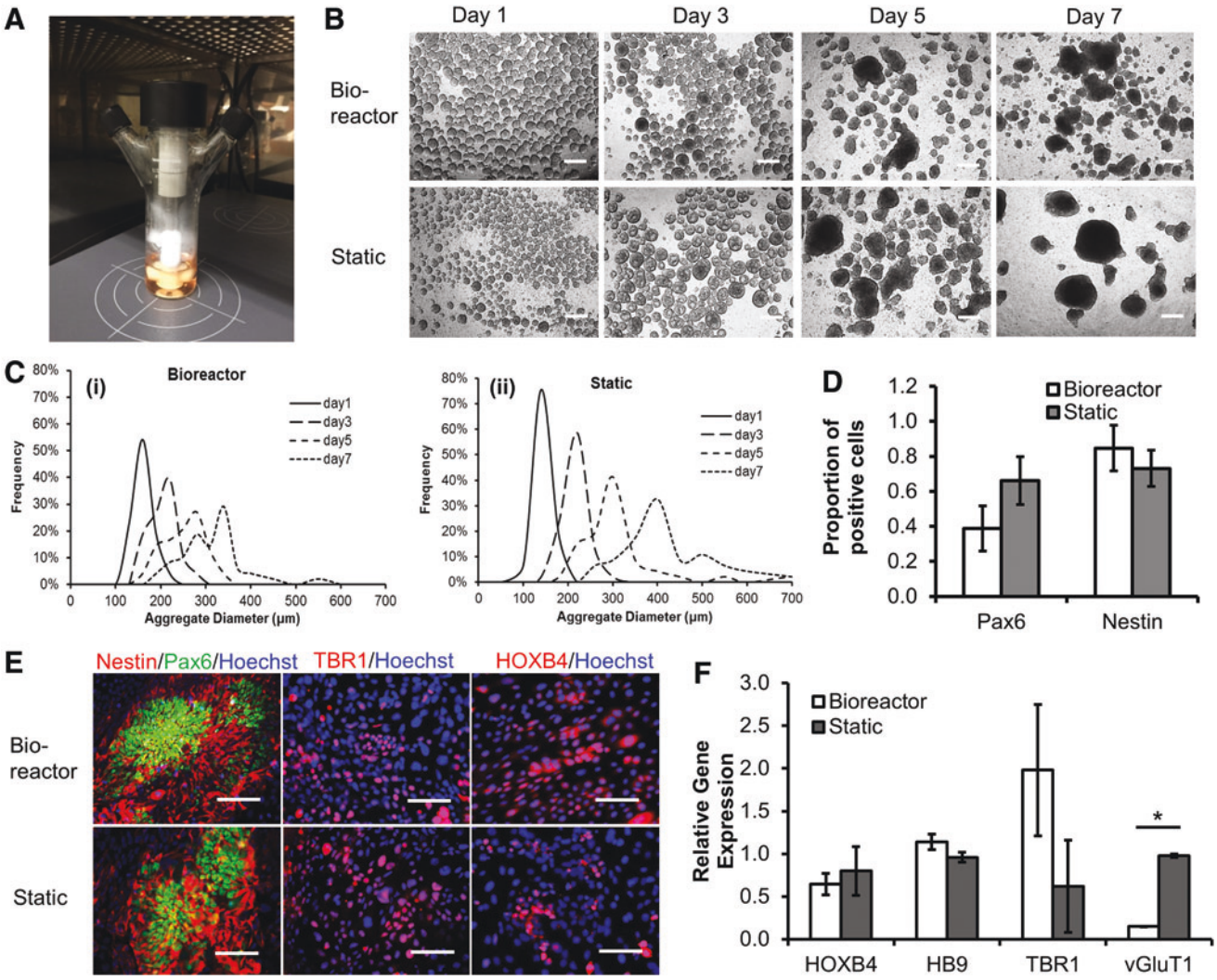

FIG. 1. Short-term bioreactor culture for no growth factor induction. **(A)** The setup of bioreactor culture. **(B)** Phase contrast images of aggregates from bioreactor culture and static culture over 7 days. Scale bar: 200 μm. **(C)** Aggregate size distribution of (i) bioreactor culture and (ii) static culture ($n = 45$–48). **(D)** Expression of Pax6 and Nestin (day 14). **(E)** Representative fluorescent images of Pax6, Nestin, TBR1, and HOXB4 ($n = 5$). Scale bar: 100 μm. **(F)** RT-PCR analysis of gene expression of *TBR1*, *vGlut1*, *HOXB4*, and *HB9* ($n = 3$). $^*p < 0.05$. RT-PCR, reverse transcription–polymerase chain reaction. Color images available online at www.liebertpub.com/tea

microscopy. The captured images were converted to binary images using ImageJ software (http://rsb.info.nih.gov/ij) and analyzed with the ''particle analysis tool.'' Through particle analysis in ImageJ software, the Feret's diameter of each aggregate in the images can be calculated, which provided the size distribution of the aggregates.

Biochemical assays: cell number and glucose/lactate assay

Cell numbers at the harvest time of bioreactor were determined using a hemocytometer after cell trypsinization of the aggregates. The supernatants were analyzed for glucose and lactate concentrations with a YSI 2700 Select™ Bioanalyzer (Yellow Spring Instruments, Yellow Spring, OH). The lactate yield from glucose (mol/mol) was calculated based on the ratio of lactate production to glucose consumption.

Bromodeoxyuridine (BrdU) assay

Briefly, the aggregates were incubated in a medium containing 10 μM BrdU (Sigma) for four hours.[34] The cells were then fixed with 70% cold ethanol, followed by a denaturation step using 2 N HCl/0.5% Triton X-100 for 30 min in the dark. The samples were reduced with 1 mg/mL sodium borohydride for 5 min and incubated with mouse anti-BrdU (1:100; Life Technologies) in a blocking buffer (0.5% Tween 20/1% bovine serum albumin in phosphate-buffered saline [PBS]), followed by Alexa Fluor® 488 goat anti-Mouse IgG_1 (Molecular Probes). The cells were counterstained with Hoechst 33342 and viewed under a confocal microscope (Zeiss LSM 880).

Immunocytochemistry

Briefly, the samples were fixed with 4% paraformaldehyde (PFA) and permeabilized with 0.2–0.5% Triton X-100

for intracellular markers. The samples were then blocked and incubated with various mouse or rabbit primary antibodies (Supplementary Table S1; Supplementary Data are available online at www.liebertpub.com/tea). After washing, the cells were incubated with the corresponding secondary antibody: Alexa Fluor 488 goat anti-Mouse IgG or Alexa Fluor 594 goat anti-Rabbit IgG (Life Technologies). The samples were stained with Hoechst 33342 and visualized using a fluorescent microscope (Olympus IX70, Melville, NY) or a confocal microscope (Zeiss LSM 880). The images from five independent fields (800–1000 cells) were analyzed using ImageJ software. The proportion of positive cells was calculated based on the area of marker of interest normalized to the nuclei using ImageJ analysis, indicating the relative expression among different conditions.

Flow cytometry

To quantify the levels of various marker expressions, the cells from the bioreactor and static control were harvested by trypsinization and analyzed by flow cytometry.[35] Briefly, 1×10^6 cells per sample were fixed with 4% PFA and washed with a staining buffer (2% fetal bovine serum in PBS). The cells were permeabilized with 100% cold methanol for intracellular markers, blocked, and then incubated with primary antibodies against Nestin, PAX6, β-tubulin III, or SATB2 followed by the corresponding secondary antibody (Supplementary Table S1). The cells were acquired with BD FACSCanto™ II flow cytometer (Becton Dickinson) and analyzed against isotype controls using FlowJo software. At least 2×10^5 cells were analyzed for each sample.

RT-PCR

Total RNA was isolated from neural cell samples using the RNeasy Mini Kit (Qiagen, Valencia, CA) according to the manufacturer's protocol followed by the treatment of DNA-Free RNA Kit (Zymo, Irvine, CA). Reverse transcription was carried out using 2 μg of total RNA, anchored oligo-dT primers (Operon, Huntsville, AL), and Superscript III (Invitrogen, Carlsbad, CA) (according to the protocol of the manufacturer). Primers specific for target genes were designed using the software Oligo Explorer 1.2 (Genelink, Hawthorne, NY; Table 1). The gene β-actin was used as an endogenous control for normalization of expression levels. Real-time RT-PCR reactions were performed on an ABI7500 instrument (Applied Biosystems, Foster City, CA), using SYBR1 Green PCR Master Mix (Applied Biosystems). The amplification reactions were performed as follows: 2 min at 50°C, 10 min at 95°C, and 40 cycles of 95°C for 15 s and 55°C for 30 s, and 68°C for 30 s. Fold variation in gene expression was quantified by means of the comparative Ct method: $2^{-(C_{t\ treatment} - C_{t\ control})}$, which is based on the comparison of expression of the target gene (normalized to the endogenous control β-actin) between the bioreactor samples and static controls.

Statistical analysis

To assess the statistical significance of the experimental results, Student's *t*-test was performed on the measurements from three replicates of bioreactor and static samples. For better comparison, the data from the side-by-side differentiation for bioreactor and static culture in the same experiment were presented. The results were expressed as [mean ± standard deviation]. A p-value <0.05 was considered statistically significant.

Results

Short-term bioreactor culture for no growth factor induction and LDN/SB induction

Neural differentiation of hiPSK3 cells in the bioreactor was first evaluated for 7 days using a neural medium without any growth factor and inoculated with single hiPSK3 cell suspension (Fig. 1). On day 1, bioreactor condition had larger EB-like aggregates than static condition (both seeded at 0.42×10^6 cells/mL). With the culture time, the aggregate size in both conditions increased and the difference was not significant (Fig. 1B). The static condition had larger aggregates by day 7 than the bioreactor condition, probably due to the merge of aggregates since the bioreactor reduced the frequency of EB merging due to agitation. The size distribution of aggregates was analyzed through image analysis (Fig. 1C). By day 7, the average diameter was 301 ± 67 μm for bioreactor condition and 394 ± 100 μm for static condition (Supplementary Fig. S1A). Lower lactate (mol)/glucose (mol) ratio was observed for bioreactor culture than static culture (1.70 ± 0.01 vs. 1.94 ± 0.08) (e.g., Run 1 in Table 2 and Supplementary Fig. S1B). However, the range of lactate/glucose ratio showed large variations in different runs (e.g., Run 3 in Table 2, 2.13 ± 0.08 vs. 2.73 ± 0.04 for bioreactor vs. static). The harvested cell density (day 7) was comparable for the two conditions (e.g., $1.13–1.26\times10^6$ cells/mL in Run 1 of Table 3). Variations from different runs were observed (e.g., $0.79–0.83\times10^6$ cells/mL for Run 2). If cell source was not good, no good aggregates were formed (data not shown). The aggregates were harvested and replated for another 7 days. The expression of Nestin and PAX6 was similar for both conditions

Table 1. Primer Sequence for Target Genes

Gene	*Forward primer 5′ to 3′*	*Reverse primer 5′ to 3′*
TBR1	CCCCCTCGTCTTTCTCTTACC	TAATGTGGAGGCCGAGACTTG
HOXB4	AATTCCTTCTCCAGCTCCAAGA	CCTGGATGCGCAAAGTTCA
vGluT1	CCCCAATTCCTCGCACTTTAT	GGGAAGGATCCCAGATTTTGA
MNX1 (HB9)	GCACCAGTTCAAGCTCAACA	TTTGCTGCGTTTCCATTTC
MMP2	CATCGCTCAGATCCGTGGTG	GCATCAATCTTTTCCGGGAGC
MMP3	CCATCTCTTCCTTCAGGCGT	ATGCCTCTTGGGTATCCAGC
Beta-actin	GTACTCCGTGTGGATCGGCG	AAGCATTTGCGGTGGACGATGG

Table 2. The Ratio of Lactate Production to Glucose Consumption

Neural induction method	*No growth factor*		*LDN/SB induction*	
Time	*Bioreactor*	*Static*	*Bioreactor*	*Static*
Run 1				
Day 1	1.61 ± 0.01	2.03 ± 0.04	1.32 ± 0.02	1.89 ± 0.04
Day 3	1.71 ± 0.02	1.96 ± 0.02	1.60 ± 0.03	2.05 ± 0.02
Day 5	1.71 ± 0.04	1.87 ± 0.01	1.58 ± 0.04	2.18 ± 0.05
Day 7	1.69 ± 0.03	1.88 ± 0.05	1.83 ± 0.01	2.28 ± 0.01
Average	1.70 ± 0.01[a]	1.94 ± 0.08[a]	1.58 ± 0.21[b]	2.10 ± 0.17[b]
Run 2				
Day 1	2.42	2.75	1.28 ± 0.01	1.99 ± 0.02
Day 3	1.79	2.04	1.51 ± 0.02	2.09 ± 0.05
Day 5	1.34	2.51	1.50 ± 0.02	2.17 ± 0.01
Day 7	1.34	2.18	1.91 ± 0.05	2.19 ± 0.02
Average	1.72 ± 0.51[a]	2.37 ± 0.32[a]	1.55 ± 0.26[b]	2.11 ± 0.09[b]
Run 3				
Day 4	2.09 ± 0.24	2.26 ± 0.03	(day 1) 1.41	(day 1) 1.85
Day 5	2.09 ± 0.01	3.04 ± 0.21	(day 3) 1.54	(day 3) 2.63
Day 6	2.23 ± 0.23	2.81 ± 0.14	1.41	2.03
Day 7	2.09 ± 0.05	2.19 ± 0.02	1.90	1.77
Average	2.13 ± 0.08[a]	2.73 ± 0.04[a]	1.57 ± 0.23[b]	2.07 ± 0.39[b]

[a]Statistical difference (p-value <0.05) between bioreactor and static cultures for no growth factor method.
[b]Statistical difference (p-value <0.05) between bioreactor and static cultures for LDN/SB induction method.

(Fig. 1D, E). The cells also expressed patterning marker TBR1 (a forebrain layer VI cortical marker) and HOXB4 (a hindbrain/spinal cord marker) (Fig. 1E). RT-PCR analysis for *HOXB4*, *HB9* (motor neuron marker), *TBR1*, and *vGluT1* (a glutamatergic neuron marker) showed higher TBR1 expression and lower vGluT1 expression for bioreactor culture than static culture (Fig. 1F). The expression of HOXB4 and HB9 was comparable.

Then, the neural differentiation was induced using LDN193189 and SB431542 for 7 days and inoculated with single cell suspension (Fig. 2). Similarly, on day 1, bioreactor condition had larger size of aggregates than static condition, but the difference was not significant at later time points. With time, the aggregate size increased and the static condition had larger aggregates by day 7 than the bioreactor condition (274 ± 122 μm vs. 416 ± 164 μm) (Fig. 2A and Supplementary Fig. S2). The lactate (mol)/glucose (mol) ratio for the bioreactor culture was lower than the static culture (1.58 ± 0.21 vs. 2.10 ± 0.17) (e.g., Run 1 in Table 2, similar observation was found for additional runs) and the harvested cell density (day 7) was comparable (0.65–0.89 × 10^6 cells/mL) (Table 3). The harvested aggregates were replated for neural marker analysis (Fig. 2B). The cells expressed patterning markers of Nestin, PAX6, TBR1m, and HOXB4, as well as the more mature neural marker β-tubulin III (Fig. 2C, D). The quantification results showed higher PAX6 and TBR1 expression for bioreactor culture than static culture, but no difference in Nestin and HOXB4 expression was observed at this time point (Fig. 2B, C), showing the influence of culture system on some neuronal markers. The expression of β-tubulin III was comparable (41–46%), evaluated at 10 days after replating of day 7 aggregates (Fig. 2D). These results indicate that bioreactor culture may alter the expression of forebrain patterning markers.

Long-term bioreactor culture for single cell inoculation

Prolonged neural differentiation to generate cortical spheroids was then performed for 21 days in the bioreactor in the presence of LDN193189 and SB431542 (Fig. 3A).

Table 3. Harvested Cell Density of the Bioreactor and Static Cultures

Runs	*Run 1*		*Run 2*		*Run 3*	
Parameters	*Bioreactor*	*Static*	*Bioreactor*	*Static*	*Bioreactor*	*Static*
No growth factor						
Day 0 seeding density (× 10^6 cells/mL)	0.42 ± 0.02	0.42 ± 0.02	0.43 ± 0.02	0.43 ± 0.02	0.42 ± 0.02	0.42 ± 0.02
Day 7 harvesting density (× 10^6 cells/mL)	1.13 ± 0.04	1.26 ± 0.04	0.79 ± 0.02	0.83 ± 0.03	0.81 ± 0.02	0.88 ± 0.02
LDN/SB induction						
Day 0 seeding density (× 10^6 cells/mL)	0.40 ± 0.01	0.40 ± 0.01	0.43 ± 0.02	0.43 ± 0.02	0.42 ± 0.02	0.42 ± 0.02
Day 7 harvesting density (× 10^6 cells/mL)	0.81 ± 0.03	0.85 ± 0.02	0.65 ± 0.03	0.73 ± 0.02	0.80 ± 0.02	0.89 ± 0.02
LDN/SB induction						
Day 0 seeding density (× 10^6 cells/mL)	0.40 ± 0.02	0.40 ± 0.02	0.40 ± 0.01	0.40 ± 0.01	0.45 ± 0.01	0.45 ± 0.01
Day 21 harvesting density (× 10^6 cells/mL)	1.24 ± 0.06	1.38 ± 0.02	0.93 ± 0.03	0.98 ± 0.02	1.29 ± 0.06	1.35 ± 0.06

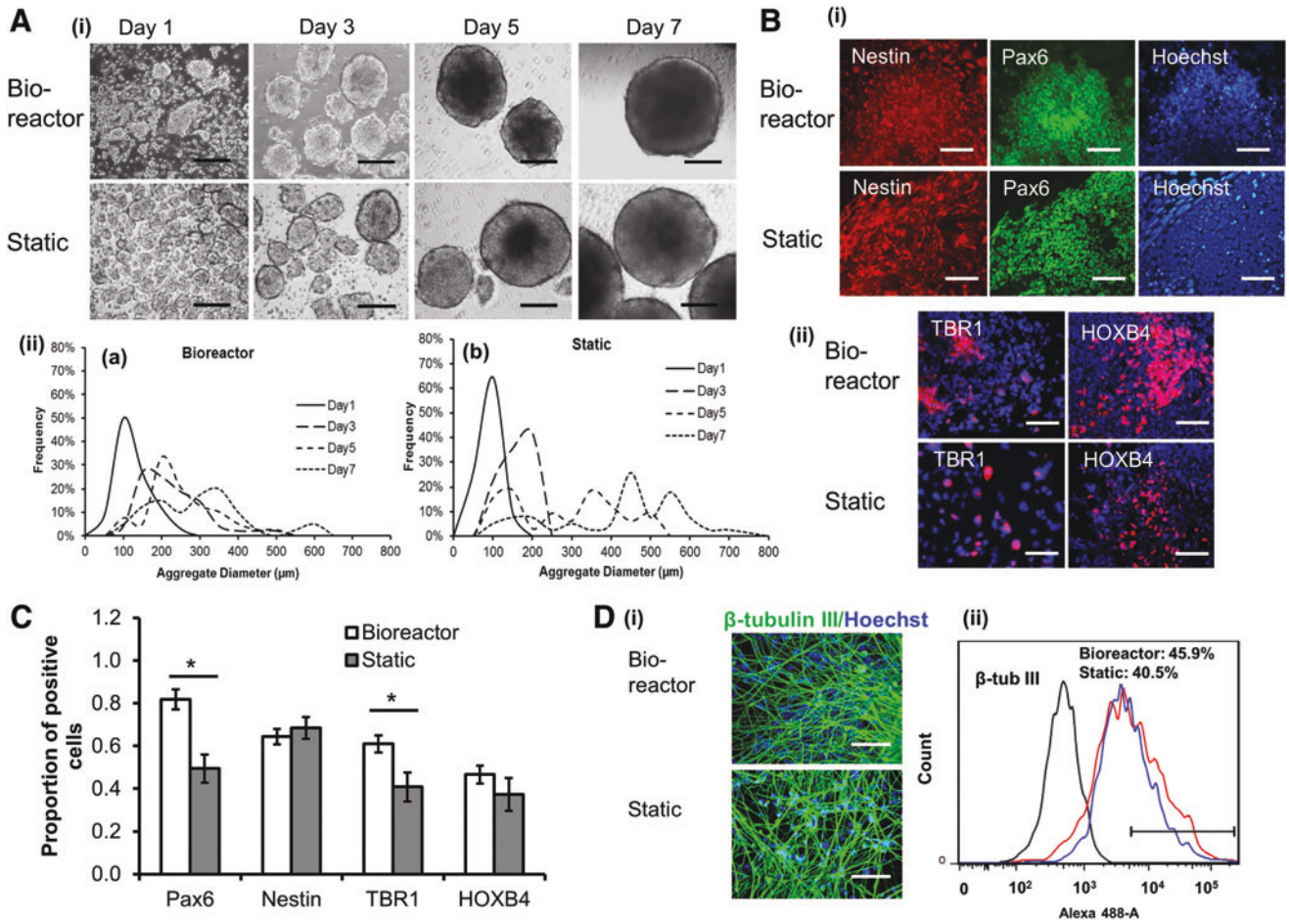

FIG. 2. Short-term bioreactor culture for LDN/SB induction. **(A)** Characterization of aggregate kinetics. (i) Phase contrast images of aggregates from bioreactor culture and static culture over 7 days. Scale bar: 200 μm. (ii) Aggregate size distribution of (a) bioreactor culture and (b) static culture ($n = 31$–48). The day 7 aggregates from bioreactor culture and static culture were replated and characterized (day 14). **(B)** Representative fluorescent images of Pax6 and Nestin (i) and the neural patterning markers TBR1 and HOXB4 (ii). Scale bar: 100 μm. **(C)** Quantification of neural marker expression ($n = 3$). **(D)** (i) Representative fluorescent images of β-tubulin III. Scale bar: 100 μm. (ii) Representative flow cytometry histogram for β-tubulin III. $*p < 0.05$. Color images available online at www.liebertpub.com/tea

With the increased culture time, the aggregate size increased, and the bioreactor condition had larger aggregates than the static condition after day 10 (Fig. 3B, C). By day 21, the average diameter was 1047 ± 174 μm for bioreactor condition and 803 ± 167 μm for static condition (Supplementary Fig. S3). The harvested cell density (day 21) was 0.93–1.38×10^6 cells/mL for bioreactor culture and static culture (Table 3). The structure of cortical spheroids (day 21) was evaluated by confocal microscopy (Fig. 4Ai). The expression of TBR1 was observed in the spheroids, but the expression of SATB2 (a marker for superficial cortical II–IV layer) was minimal. The aggregates also expressed HOXB4 and β-tubulin III. The expression of presynaptic marker synapsin I and postsynaptic marker PSD95 was observed (day 28) (Fig. 4Aii). RT-PCR analysis showed higher *HOXB4* and *TBR1* expression, but lower *vGluT1* expression for bioreactor culture than static culture (Fig. 4B). Gene expression of matrix metalloproteinase (MMP)-2 and −3 was evaluated to show the influence of culture environment on matrix remodeling (Fig. 4C and Supplementary Fig. S4). *MMP-2* expression was lower, but *MMP-3* expression was higher for bioreactor culture than static culture. These results demonstrate the development of early stage cortical spheroids from hiPSCs, and bioreactor culture increased the gene expression of *HOXB4* and *TBR1* and altered *MMP-2/-3* expression.

Long-term bioreactor culture for EB inoculation

To evaluate if the exposure to bioreactor culture has a temporal effect, the bioreactor was inoculated with day 8 EBs after the ectoderm induction by dual SMAD inhibitors (Fig. 5A). With the increased culture time, the aggregate size increased. The bioreactor condition had larger aggregates than static condition, probably due to better nutrient diffusion (Fig. 5B, C). By day 27, the average diameter was 1121 ± 91 μm for bioreactor condition and 997 ± 152 μm for static condition (Supplementary Fig. S3). The replated spheroids expressed cortical markers of TBR1 and glutamate, as well as synaptic markers synapsin I and PSD95 (Fig. 6A). HOXB4 expression was also visible. RT-PCR analysis showed higher *HOXB4* and *TBR1* expression, but

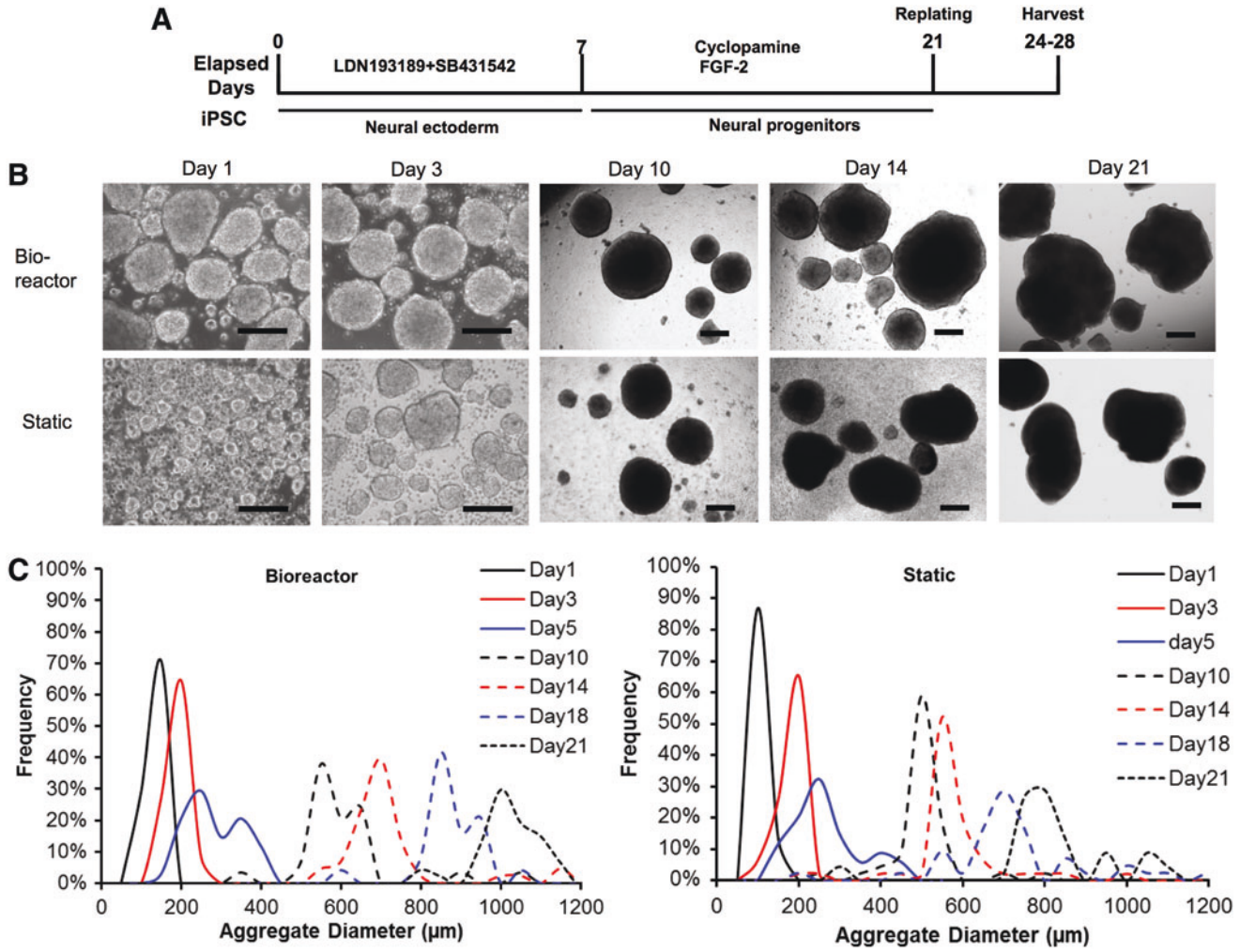

FIG. 3. Long-term bioreactor culture for single cell inoculation—aggregate characterization. **(A)** Schematic illustration of cortical spheroid development from hiPSK3 cells in a bioreactor culture, inoculated with single undifferentiated hiPSK3 cells. **(B)** Phase contrast images of aggregates from bioreactor culture and static culture over 21 days. Scale bar: 200 μm. **(C)** Aggregate size distribution of bioreactor culture and static culture ($n = 34$–48). Color images available online at www.liebertpub.com/tea

slightly lower *vGluT1* expression for bioreactor culture than static culture (Fig. 6B). The expression of SATB2 (day 32) showed 37% for bioreactor culture and 14% for static culture (Fig. 6C. In Supplementary Fig. S5, SATB2 is 32 ± 15% for bioreactor and 13 ± 2% for static culture). High expression of β-tubulin III (78–92%) was observed for both cultures. These data indicate that bioreactor culture increases the expression of TBR1, SATB2, and HOXB4 at the neural patterning stage after day 8 of ectoderm induction.

Characterization of long-term cortical spheroids derived from hiPSCs

Long-term culture of cortical spheroids in bioreactor inoculated with the preformed EBs was performed (Fig. 7). The structure of cortical spheroids was evaluated by confocal microscopy for the expression of TBR1 and SATB2 (Fig. 7A). While SATB2 expression appeared on day 43, no clear layer structure was observed. The expression of β-tubulin III was around 88–89% for both cultures (Fig. 7B), distributed throughout the spheroids (Supplementary Fig. S6). The expression of SATB2 was 40.1% for bioreactor and 50.6% for static culture on day 44, indicating that static culture reached the similar level of SATB2 expression after a longer culture period (Fig. 7B). Another superficial layer II–IV marker BRN2 (layer III) was observed on day 48 (Fig. 7C). Prolonged culture was performed up to day 71 and the layered cortical structure was more visible (Fig. 7D), with a specific superficial layer of $SATB2^+$ cells formed next to the deep layer of $TBR1^+$ cells. The expression of TBR1 and SATB2/BRN2 at different time points demonstrates that the cortical spheroids followed ''inside-out'' developmental pattern of human cortex (Supplementary Fig. S7). Moreover, co-localization of BRN2 and BrdU was observed, indicating the proliferation capability of superficial layer cells (Fig. 7E). By contrast, TBR1 and BrdU expression were not co-localized, indicating the formation of deep layer cells at the early stage of development before the appearance of superficial layer cells.[2] These results demonstrate the formation of layer-specific structure of cortical spheroids from hiPSCs in a long-term culture.

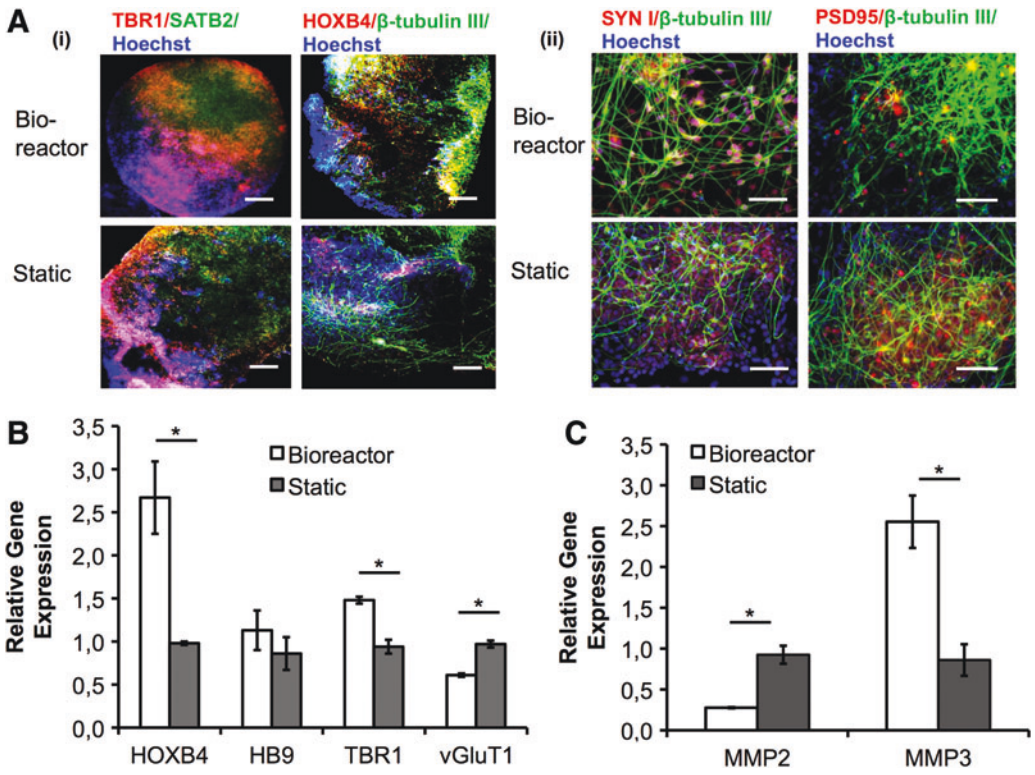

FIG. 4. Long-term bioreactor culture for single cell inoculation—neural differentiation characterization. The day 21 aggregates from bioreactor culture and static culture were harvested and characterized. **(A)** (i) Confocal images of TBR1(*red*)/SATB2(*green*)/Hoechst(*blue*) expression and HOXB4(*red*)/β-tubulin III(*green*)/Hoechst(*blue*) expression in the spheroids (day 25) derived from bioreactor culture and static culture. Scale bar: 200 μm. The aggregates were replated for another 7 days for synaptic marker expression. (ii) The expression of presynaptic marker Synapsin I (SYN I) and post-synaptic marker PSD95 (day 28). Scale bar: 100 μm. **(B)** RT-PCR analysis of gene expression of *TBR1*, *vGlut1*, *HOXB4*, and *HB9* (day 21) ($n=3$). **(C)** RT-PCR analysis of gene expression of *MMP2* and *MMP3* (day 21) ($n=3$). *$p<0.05$. MMP, matrix metalloproteinase. Color images available online at www.liebertpub.com/tea

Additional characterizations confirmed the expression of cortical markers BRN2 and TBR1 (Supplementary Fig. S8A). GABAergic interneurons were also observed based on the expression of GABA and vGAT (about 15–20%) (Supplementary Fig. S8B). In addition, mature neuron markers MAP-2 and tau, the microtubule-associated proteins involved in pathological development of various neurological diseases,[36,37] were expressed in the replated spheroids (Supplementary Fig. S8C). The cell populations also have some astrocytes indicated by the expression of GFAP (Supplementary Fig. S8D). These data further indicate the cortical tissue properties of the derived spheroids.

Discussion

Recent developments in recapitulating neurodegenerative diseases and the findings of differential susceptibility of different neuronal subtypes demonstrate the critical needs for novel *in vitro* brain-like tissue models for disease modeling and drug screening.[13,14,38–40] Forebrain cortical neurons, spheroids, and organoids have wide applications in neurological disorders, including Alzheimer's disease, microcephaly, brain injury, and stroke.[2,9,18,41] Human cortex has six layers with the deep layer VI neurons ($TBR1^+$ early-born neurons) being generated first and the superficial layer II–IV neurons ($SATB2^+$ late-born neurons) appearing later,[42] following an ''inside-out'' developmental pattern.[43] However, the brain-like tissue models not only need to contain relevant cell populations but also the 3D organization of appropriate structure. The forebrain-like 3D cortical tissue development from hPSCs has been investigated *in vitro* in static culture environment.[28,42,44] Comparison of 3D aggregate-based neural differentiation with 2D monolayer differentiation showed that aggregate-based neural differentiation resulted in higher $MAP\text{-}2^+$ cells (93% vs. 45% at day 40).[45]

Despite rapid development of *in vitro* generation of 3D mini-brain or organoid models from hPSCs, the size and the complexity of the neural structures are limited by the culture systems and inadequate supply of nutrients and oxygen.[46] Bioreactors can enhance the diffusion of biomolecules and patterning factors and were used for generating large size of organoids in a couple of studies,[10,18] but the exact role of bioreactor system in brain organoid development remains unknown. Our study indicates that bioreactor culture promotes the expression of TBR1 (a forebrain cortical layer marker) and HOXB4 (a hindbrain/spinal cord marker), affecting neural tissue patterning in brain spheroids/organoids derived from hiPSCs.

The bioreactor culture has some possible effects on cortical tissue development based on our results. On one hand, the dynamic culture environment exposes shear stress to the surface of the aggregates, which causes signal transduction

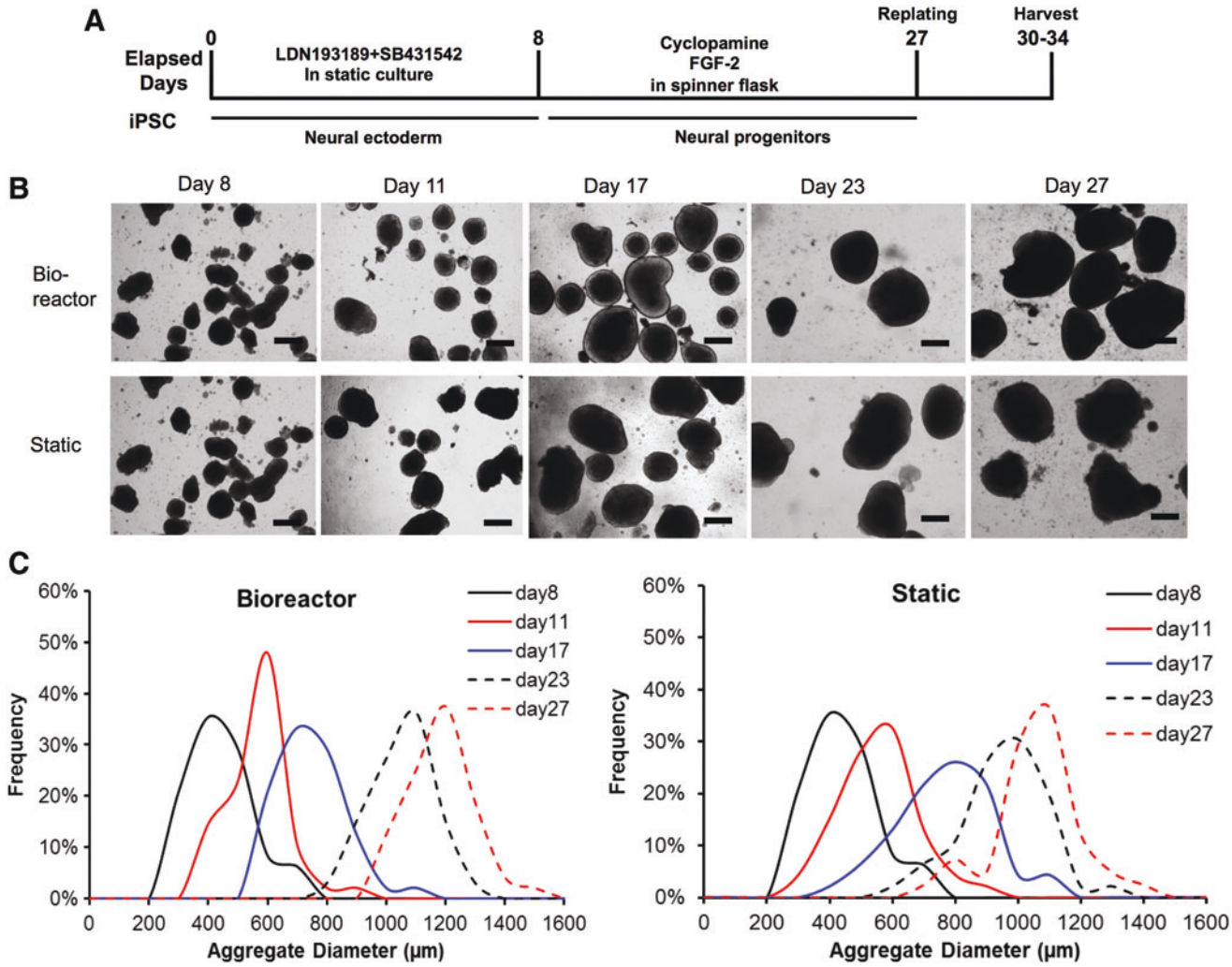

FIG. 5. Long-term bioreactor culture for EB inoculation—aggregate characterizations. **(A)** Schematic illustration of cortical spheroid development from hiPSK3 cells in a bioreactor culture, inoculated with day 8 EBs. **(B)** Phase contrast images of aggregates from bioreactor culture and static culture over 27 days. Scale bar: 400 μm. **(C)** Aggregate size distribution of bioreactor culture and static culture ($n = 33–48$). EBs, embryoid bodies. Color images available online at www.liebertpub.com/tea

of mechanical forces, leading to the activation of intracellular pathways such as Wnt (Supplementary Fig. S9),[26,27] which may contribute to the upregulation of HOXB4.[47] On the other hand, the dynamic culture environment enhances the diffusion of neural patterning factors (e.g., cyclopamine), nutrients, and oxygen and promotes cortical tissue development,[48,49] which may contribute to the upregulation of TBR1.

Based on the geometry of the bioreactor used in this study, the estimated maximum shear stress is 2.3–3.4 dyne/cm^2,[50] although most spheroids would not experience the impeller maximum shear stress. Shear stress in bioreactors alters the kinetics of ligand-receptor binding and changes the frequency of cell collision, which may also lead to altered cell phenotype.[25,51] The fluidic pattern in a spinner bioreactor shows the maximum flow velocity at the edge of the impeller, and the lowest flow velocity in the center under the impeller based on our computational fluidic dynamics (CFD) analysis (Supplementary Fig. S10),[52] which contributes to the heterogeneity of aggregate size. The detailed analysis of predicting the actual stresses experienced by the spheroids needs more complex CFD analysis to be performed in future.

In addition, bioreactor culture alters the concentration gradients inside the aggregates in a more controllable way[48,49] and thus may exert differential impact on neural patterning from hPSCs compared to static culture. For example, the sonic hedgehog (Shh) antagonist cyclopamine would show a deeper penetration into the aggregates for bioreactor culture than static culture, influencing the ventralization process; so the inhibition of Shh may enhance forebrain cortical marker TBR1 expression. Moreover, bioreactor culture enhances oxygen diffusion, which plays a role in cell metabolism. Further studies are required to establish the direct correlation of oxygen and/or other metabolic state factors with cortical tissue development. These differences in culture environment may collectively contribute to the difference of cortical tissue development from hiPSCs between the bioreactor culture and static culture.

The bioreactor culture of day 8 preformed EBs also showed the elevated gene expression of HOXB4 and TBR1,

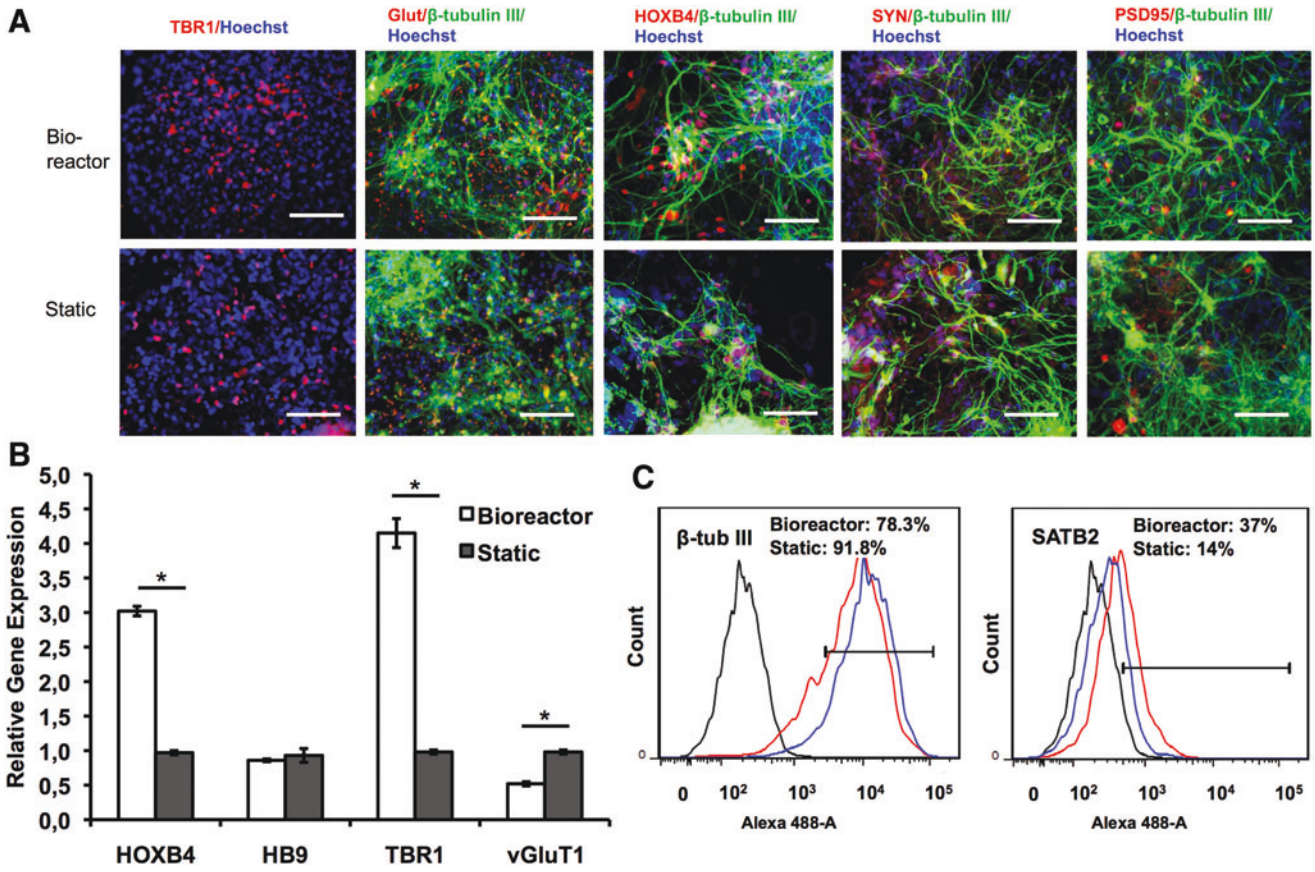

FIG. 6. Long-term bioreactor culture for EB inoculation—neural differentiation characterization. On day 27, aggregates from bioreactor and static cultures were replated and characterized. **(A)** Representative fluorescent images of TBR1, HOXB4, glutamate, and the expression of presynaptic marker synapsin I and postsynaptic marker PSD95 (day 32). Scale bar: 100 μm. **(B)** RT-PCR analysis of gene expression of *TBR1*, *vGlut1*, *HOXB4*, and *HB9* (day 32) ($n=3$). **(C)** Representative flow cytometry histograms for SATB2 and β-tubulin III (day 30). $*p<0.05$. Color images available online at www.liebertpub.com/tea

indicating that the temporal exposure to dynamic culture environment is important during neural patterning stage (day 8–15) rather than neural ectoderm induction stage (day 0–7). Neural patterning stage involves multiple signaling pathways to modulate the regional specificity of brain tissue along anterior-posterior (A-P) axis and dorsal-ventral (D-V) axis.[53,54] It was thought that the gradients of signaling molecules during neural patterning stage play a critical role in spatially defining the neuronal subtypes in the 3D neural spheroids/organoids.[54]

Besides the bulk fluid dynamic environment, it was thought that the interstitial flow (0.1–1.0 dyne/cm^2) inside the aggregates may play an important role in tissue morphogenesis and development.[55] The parenchymal cells of brain are surrounded by interstitial fluid.[56] Regulation of the fluid composition and volume is achieved by the barriers between central nervous system and blood. The interstitial space is usually occupied by ECMs, which determine the resistance to fluid flow. Therefore, interstitial flow is very slow and generates low levels of shear stress. Besides enhancing nutrient diffusion, the interstitial flow affects ECM deposition and cytokine production from the cells. Shear stress at interstitial levels (0.135 dyne/cm^2) may affect the nuclear localization of transcriptional coactivator with PDZ binding motif (TAZ),[57] an effector protein and signaling mediator of mechanotransduction along with Yes-associated protein,[58,59] which could impact cellular differentiation.[57]

Based on the knowledge of interstitial flow, it is speculated that stirred agitation in a spinner bioreactor may provide interstitial flow inside the aggregates that is felt by the cells and promotes nutrient diffusion in our study. The embryonic stem cell (ESC) aggregate porosity (or void space) is estimated to be about 0.26–0.48.[48,60] If the aggregate surface experiences 3–15 dyne/cm^2 (the range of blood flow shear), the flow penetration into the aggregates (tissue-like structure) would be at the interstitial level (0.1–0.2 dyne/cm^2) due to the resistance from ECMs among the cells in the aggregates.[55] Such interstitial flow would be minimal in static culture. It is possible that the interstitial flow inside the aggregates of bioreactor culture contributes to the alter expression of neural patterning makers (TBR1 and HOXB4) observed in this study.

The results from this study indicate that MMP-2 and MMP-3 expression can be altered by the culture system. MMP-2 expression was slightly decreased, while MMP-3 expression was increased in bioreactor culture compared to static culture. MMP-2, also known as gelatinase A, mainly degrades type IV collagen, the most abundant basement

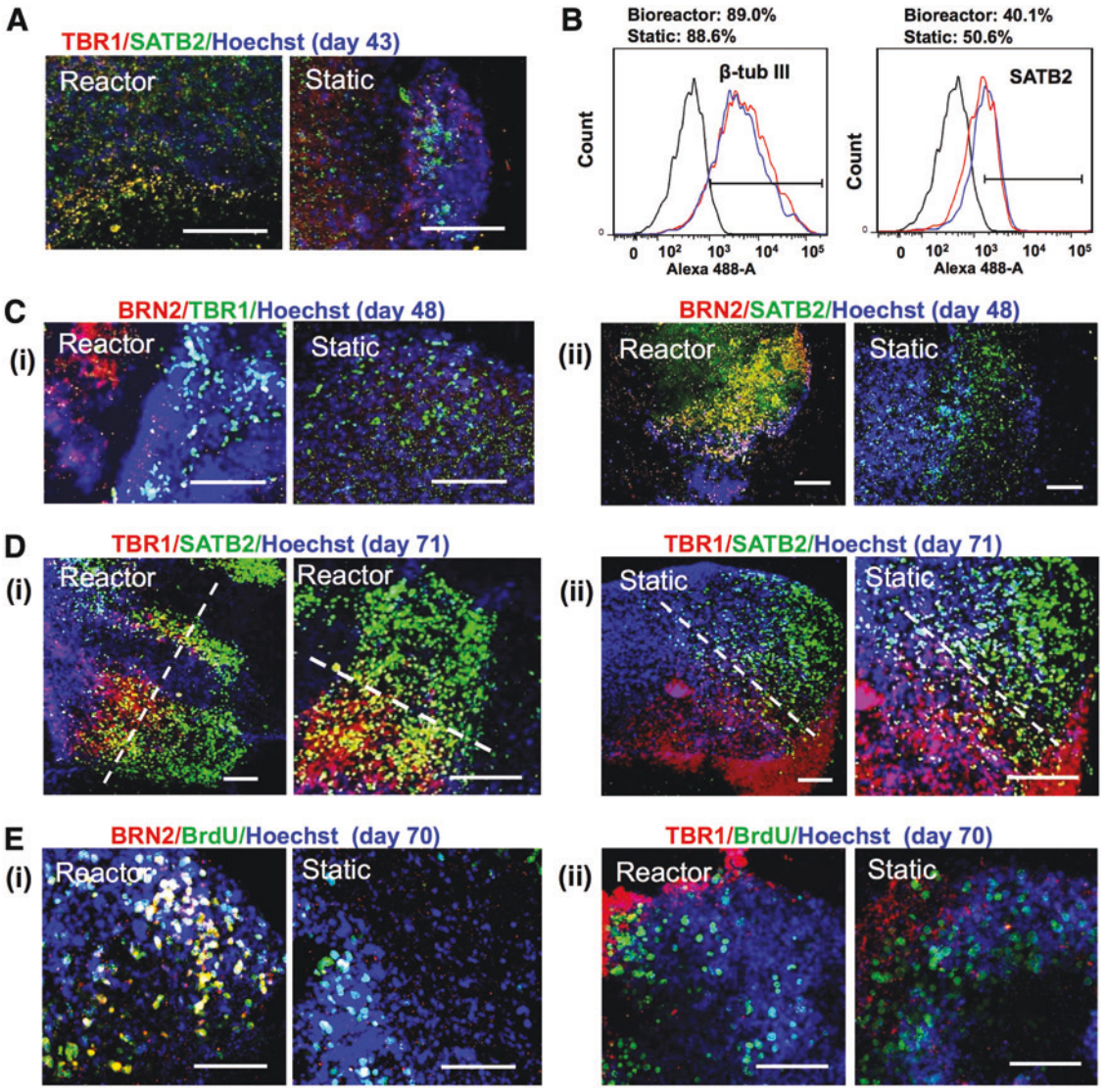

FIG. 7. Layer-specific structural characterizations of long-term cortical spheroids derived from human induced pluripotent stem cells. **(A)** Confocal images of TBR1/SATB2/Hoechst expression in the spheroids (day 43) derived from bioreactor culture and static culture. **(B)** Representative flow cytometry histogram for SATB2 and β-tubulin III (day 44). **(C)** Confocal images of spheroids with cortical layer-specific markers (TBR1-layer VI, BRN2-layer III, and SATB2-layer IV on day 48). (i) BRN2/TBR1/Hoechst; (ii) BRN2/SATB2/Hoechst. **(D)** Confocal images of spheroids with cortical layer-specific markers (TBR1 and SATB2 on day 71); (i) bioreactor culture; (ii) static culture. **(E)** Confocal images of spheroids with localization of BrdU expression and cortical layer-specific markers (TBR1 and BRN2 at day 70). (i) BRN2/BrdU/Hoechst; (ii) TBR1/BrdU/Hoechst. Scale bar: 100 μm. Color images available online at www.liebertpub.com/tea

membrane protein.[61] MMP-3, also known as stromelysin-1, degrades collagen types II, III, IV, IX, and X, proteoglycans, fibronectin, laminin, and elastin. MMP-3 is also an activator for pro-MMP-9, which regulates MMP-9 activity.[62] MMP-3 deficiency has been shown to result in the delayed granule cell radial migration and disturbance in synaptogenesis in Purkinje cells of cerebellar cortex.[63,64] Our study demonstrates the effect of dynamic culture on forebrain-like cortical tissue development from hiPSCs by temporally modulating ECM remodeling proteins. The dynamic culture of ESC aggregates has been shown to modulate the ECM (e.g., laminin) and growth factor (e.g., bone morphogenetic protein 4) expression pattern compared to static culture, during the development of mesodermal lineages.[65] The ECMs in brain tissues consist of basement membrane proteins (e.g., laminin, fibronectin, collagen IV, and heparan sulfate proteoglycans), perineuronal nets (e.g., hyaluronic acid and chondroitin sulfate proteoglycans), and interstitial matrix (e.g., laminin and tenascin R).[66,67] Investigation of ECM remodeling and composition affected by the culture systems may reveal the mechanisms of brain tissue memory and neurological disease progression, which needs further study.

It shall be noted that the reported system in the current form cannot fully address the robustness in the production of spheroids. Large variations exist in metabolic activity and aggregate size, where cell source may also play a role. In the future, several strategies may be explored to address the issues related to the variability in spheroid/organoid

production. For examples, controlled input cell population and defined matrix components may be used together with optimized feeding strategy. They may help reduce the spheroid-spheroid or organoid-organoid variability and improve the reproducibility of the experimental systems.

Conclusions

This study indicates that bioreactor culture alters the expression of neural patterning markers during the cortical spheroid formation from hiPSCs compared to static culture. The results demonstrate the importance of culture environment in cortical tissue development from hiPSCs during the establishment of *in vitro* 3D brain-like tissue models. This study has significance in deriving brain organoids from hPSCs for disease modeling and drug discovery.

Acknowledgments

The authors would like to thank Ms. Ruth Didier in FSU Department of Biomedical Sciences for her help with flow cytometry analysis, Dr. Brian K. Washburn and Kristina Poduch in FSU Department of Biological Sciences for their help with RT-PCR analysis, Dr. Stephen Duncan at Medical College of Wisconsin and Dr. David Gilbert in FSU Department of Biological Sciences for human iPSK3 cells, and Dr. Ravindran Chella of FSU Department of Chemical and Biomedical Engineering for his help in CFD analysis. This work is supported by FSU start up fund, FSU Bridge Fund, and National Science Foundation (Grant No. 1652992).

Disclosure Statement

No competing financial interests exist.

References

1. Choi, S.H., Kim, Y.H., Hebisch, M., Sliwinski, C., Lee, S., D'Avanzo, C., Chen, H., Hooli, B., Asselin, C., Muffat, J., Klee, J.B., Zhang, C., Wainger, B.J., Peitz, M., Kovacs, D.M., Woolf, C.J., Wagner, S.L., Tanzi, R.E., and Kim, D.Y. A three-dimensional human neural cell culture model of Alzheimer's disease. Nature **515,** 274, 2014.
2. Pasca, A.M., Sloan, S.A., Clarke, L.E., Tian, Y., Makinson, C.D., Huber, N., Kim, C.H., Park, J.Y., O'Rourke, N.A., Nguyen, K.D., Smith, S.J., Huguenard, J.R., Geschwind, D.H., Barres, B.A., and Pasca, S.P. Functional cortical neurons and astrocytes from human pluripotent stem cells in 3D culture. Nat Methods **12,** 671, 2015.
3. Simao, D., Pinto, C., Piersanti, S., Weston, A., Peddie, C.J., Bastos, A.E., Licursi, V., Schwarz, S.C., Collinson, L.M., Salinas, S., Serra, M., Teixeira, A.P., Saggio, I., Lima, P.A., Kremer, E.J., Schiavo, G., Brito, C., and Alves, P.M. Modeling human neural functionality in vitro: three-dimensional culture for dopaminergic differentiation. Tissue Eng Part A **21,** 654, 2015.
4. Schwartz, M.P., Hou, Z.; Propson, N.E., Zhang, J., Engstrom, C.J., Costa, V.S., Jiang, P., Nguyen, B.K., Bolin, J.M., Daly, W., Wang, Y., Stewart, R., Page, C.D., Murphy, W.L., and Thomson, J.A. Human pluripotent stem cell-derived neural constructs for predicting neural toxicity. Proc Natl Acad Sci U S A **112,** 12516, 2015.
5. Hill, R.S., and Walsh, C.A. Molecular insights into human brain evolution. Nature **437,** 64, 2005.
6. Choi, Y.J., Park, J., and Lee, S.H. Size-controllable networked neurospheres as a 3D neuronal tissue model for Alzheimer's disease studies. Biomaterials **34,** 2938, 2013.
7. Engle, S.J., and Puppala, D. Integrating human pluripotent stem cells into drug development. Cell Stem Cell **12,** 669, 2013.
8. Grskovic, M., Javaherian, A., Strulovici, B., and Daley, G.Q. Induced pluripotent stem cells—opportunities for disease modelling and drug discovery. Nat Rev Drug Discov **10,** 915, 2011.
9. Vazin, T., Ball, K.A., Lu, H., Park, H., Ataeijannati, Y., Head-Gordon, T., Poo, M.M., and Schaffer, D.V. Efficient derivation of cortical glutamatergic neurons from human pluripotent stem cells: a model system to study neurotoxicity in Alzheimer's disease. Neurobiol Dis **62,** 62, 2014.
10. Lancaster, M.A., Renner, M., Martin, C.A., Wenzel, D., Bicknell, L.S., Hurles, M.E., Homfray, T., Penninger, J.M., Jackson, A.P., and Knoblich, J.A. Cerebral organoids model human brain development and microcephaly. Nature **501,** 373, 2013.
11. Vogel, G. Neurodevelopment. Lab dishes up mini-brains. Science **341,** 946, 2013.
12. Israel, M.A., Yuan, S.H., Bardy, C., Reyna, S.M., Mu, Y., Herrera, C., Hefferan, M.P., Van Gorp, S., Nazor, K.L., Boscolo, F.S., Carson, C.T., Laurent, L.C., Marsala, M., Gage, F.H., Remes, A.M., Koo, E.H., and Goldstein, L.S. Probing sporadic and familial Alzheimer's disease using induced pluripotent stem cells. Nature **482,** 216, 2012.
13. Kondo, T., Asai, M., Tsukita, K., Kutoku, Y., Ohsawa, Y., Sunada, Y., Imamura, K., Egawa, N., Yahata, N., Okita, K., Takahashi, K., Asaka, I., Aoi, T., Watanabe, A., Watanabe, K., Kadoya, C., Nakano, R., Watanabe, D., Maruyama, K., Hori, O., Hibino, S., Choshi, T., Nakahata, T., Hioki, H., Kaneko, T., Naitoh, M., Yoshikawa, K., Yamawaki, S., Suzuki, S., Hata, R., Ueno, S., Seki, T., Kobayashi, K., Toda, T., Murakami, K., Irie, K., Klein, W.L., Mori, H., Asada, T., Takahashi, R., Iwata, N., Yamanaka, S., and Inoue, H. Modeling Alzheimer's disease with iPSCs reveals stress phenotypes associated with intracellular Abeta and differential drug responsiveness. Cell Stem Cell **12,** 487, 2013.
14. Yin, X., Mead, B.E., Safaee, H., Langer, R., Karp, J.M., and Levy, O. Engineering stem cell organoids. Cell Stem Cell **18,** 25, 2016.
15. Yahata, N., Asai, M., Kitaoka, S., Takahashi, K., Asaka, I., Hioki, H., Kaneko, T., Maruyama, K., Saido, T.C., Nakahata, T., Asada, T., Yamanaka, S., Iwata, N., and Inoue, H. Anti-Abeta drug screening platform using human iPS cell-derived neurons for the treatment of Alzheimer's disease. PLoS One **6,** e25788, 2011.
16. Nieweg, K., Andreyeva, A., van Stegen, B., Tanriover, G., and Gottmann, K. Alzheimer's disease-related amyloid-beta induces synaptotoxicity in human iPS cell-derived neurons. Cell Death Dis **6,** e1709, 2015.
17. Zhang, D., Pekkanen-Mattila, M., Shahsavani, M., Falk, A., Teixeira, A.I., and Herland, A. A 3D Alzheimer's disease culture model and the induction of P21-activated kinase mediated sensing in iPSC derived neurons. Biomaterials **35,** 1420, 2014.
18. Qian, X., Nguyen, H.N., Song, M.M., Hadiono, C., Ogden, S.C., Hammack, C., Yao, B., Hamersky, G.R., Jacob, F., Zhong, C., Yoon, K.J., Jeang, W., Lin, L., Li, Y., Thakor, J., Berg, D.A., Zhang, C., Kang, E., Chickering, M., Nauen, D., Ho, C.Y., Wen, Z., Christian, K.M., Shi, P.Y., Maher,

B.J., Wu, H., Jin, P., Tang, H., Song, H., and Ming, G.L. Brain-region-specific organoids using mini-bioreactors for modeling ZIKV exposure. Cell **165,** 1238, 2016.

19. Takebe, T., Sekine, K., Enomura, M., Koike, H., Kimura, M., Ogaeri, T., Zhang, R.R., Ueno, Y., Zheng, Y.W., Koike, N., Aoyama, S., Adachi, Y., and Taniguchi, H. Vascularized and functional human liver from an iPSC-derived organ bud transplant. Nature **499,** 481, 2013.
20. Miranda, C.C., Fernandes, T.G., Pascoal, J.F., Haupt, S., Brustle, O., Cabral, J.M., and Diogo, M.M. Spatial and temporal control of cell aggregation efficiently directs human pluripotent stem cells towards neural commitment. Biotechnol J **10,** 1612, 2015.
21. Frith, J.E., Thomson, B., and Genever, P.G. Dynamic three-dimensional culture methods enhance mesenchymal stem cell properties and increase therapeutic potential. Tissue Eng Part C Methods **16,** 735, 2010.
22. Sart, S., Tsai, A.-C., Li, Y., and Ma, T. Three-dimensional aggregates of mesenchymal stem cells: cellular mechanisms, biological properties, and applications. Tissue Eng Part B Rev **20,** 365, 2014.
23. Chen, V.C., Ye, J., Shukla, P., Hua, G., Chen, D., Lin, Z., Liu, J.C., Chai, J., Gold, J., Wu, J., Hsu, D., and Couture, L.A. Development of a scalable suspension culture for cardiac differentiation from human pluripotent stem cells. Stem Cell Res **15,** 365, 2015.
24. Sart, S., Agathos, S.N., Li, Y., and Ma, T. Regulation of mesenchymal stem cell 3D microenvironment: from macro to microfluidic bioreactors. Biotechnol J **11,** 43, 2016.
25. Kinney, M.A., Sargent, C.Y., and McDevitt, T.C. The multiparametric effects of hydrodynamic environments on stem cell culture. Tissue Eng Part B Rev **17,** 249, 2011.
26. Rodrigues, C.A., Fernandes, T.G., Diogo, M.M., da Silva, C.L., and Cabral, J.M. Stem cell cultivation in bioreactors. Biotechnol Adv **29,** 815, 2011.
27. Tandon, N., Marolt, D., Cimetta, E., and Vunjak-Novakovic, G. Bioreactor engineering of stem cell environments. Biotechnol Adv **31,** 1020, 2013.
28. Eiraku, M., Watanabe, K., Matsuo-Takasaki, M., Kawada, M., Yonemura, S., Matsumura, M., Wataya, T., Nishiyama, A., Muguruma, K., and Sasai, Y. Self-organized formation of polarized cortical tissues from ESCs and its active manipulation by extrinsic signals. Cell Stem Cell **3,** 519, 2008.
29. Si-Tayeb, K., Noto, F.K., Sepac, A., Sedlic, F., Bosnjak, Z.J., Lough, J.W., and Duncan, S.A. Generation of human induced pluripotent stem cells by simple transient transfection of plasmid DNA encoding reprogramming factors. BMC Dev Biol **10,** 81, 2010.
30. Si-Tayeb, K., Noto, F.K., Nagaoka, M., Li, J., Battle, M.A., Duris, C., North, P.E., Dalton, S., and Duncan, S.A. Highly efficient generation of human hepatocyte-like cells from induced pluripotent stem cells. Hepatology **51,** 297, 2010.
31. Yan, Y., Martin, L., Bosco, D., Bundy, J., Nowakowski, R., Sang, Q. X., and Li, Y. Differential effects of acellular embryonic matrices on pluripotent stem cell expansion and neural differentiation. Biomaterials **73,** 231, 2015.
32. Yan, Y., Bejoy, J., Xia, J., Guan, J., Zhou, Y., and Li, Y. Neural patterning of human induced pluripotent stem cells in 3-D cultures for studying biomolecule-directed differential cellular responses. Acta Biomater **42,** 114, 2016.
33. Yan, Y., Song, L., Tsai, A.-C., Ma, T., and Li, Y. Generation of neural progenitor spheres from human pluripotent stem cells in a suspension bioreactor. Methods Mol Biol **1502,** 119, 2016.
34. Sart, S., Yan, Y., Li, Y., Lochner, E., Zeng, C., Ma, T., and Li, Y. Crosslinking of extracellular matrix scaffolds derived from pluripotent stem cell aggregates modulates neural differentiation. Acta Biomater **30,** 222, 2016.
35. Sart, S., Ma, T., and Li, Y. Extracellular matrices decellularized from embryonic stem cells maintained their structure and signaling specificity. Tissue Eng Part A **20,** 54, 2014.
36. Ehrlich, M., Hallmann, A.L., Reinhardt, P., Arauzo-Bravo, M.J., Korr, S., Ropke, A., Psathaki, O.E., Ehling, P., Meuth, S.G., Oblak, A.L., Murrell, J.R., Ghetti, B., Zaehres, H., Scholer, H.R., Sterneckert, J., Kuhlmann, T., and Hargus, G. Distinct neurodegenerative changes in an induced pluripotent stem cell model of frontotemporal dementia linked to mutant TAU protein. Stem Cell Reports **5,** 83, 2015.
37. Bloom, G.S. Amyloid-beta and tau: the trigger and bullet in Alzheimer disease pathogenesis. JAMA Neurol **71,** 505, 2014.
38. Mertens, J., Wang, Q.W., Kim, Y., Yu, D.X., Pham, S., Yang, B., Zheng, Y., Diffenderfer, K.E., Zhang, J., Soltani, S., Eames, T., Schafer, S.T., Boyer, L., Marchetto, M.C., Nurnberger, J.I., Calabrese, J.R., Odegaard, K.J., McCarthy, M.J., Zandi, P.P., Alba, M., Nievergelt, C.M., Mi, S., Brennand, K.J., Kelsoe, J.R., Gage, F.H., and Yao, J. Differential responses to lithium in hyperexcitable neurons from patients with bipolar disorder. Nature **527,** 95, 2015.
39. Passier, R., Orlova, V., and Mummery, C. Complex tissue and disease modeling using hiPSCs. Cell Stem Cell **18,** 309, 2016.
40. Li, Y., Xu, C., and Ma, T. In vitro organogenesis from pluripotent stem cells. Organogenesis **10,** 159, 2014.
41. Tornero, D., Wattananit, S., Gronning Madsen, M., Koch, P., Wood, J., Tatarishvili, J., Mine, Y., Ge, R., Monni, E., Devaraju, K., Hevner, R.F., Brustle, O., Lindvall, O., and Kokaia, Z. Human induced pluripotent stem cell-derived cortical neurons integrate in stroke-injured cortex and improve functional recovery. Brain **136,** 3561, 2013.
42. van den Ameele, J., Tiberi, L., Vanderhaeghen, P., and Espuny-Camacho, I. Thinking out of the dish: what to learn about cortical development using pluripotent stem cells. Trends Neurosci **37,** 334, 2014.
43. Shi, Y., Kirwan, P., Smith, J., Robinson, H.P., and Livesey, F.J. Human cerebral cortex development from pluripotent stem cells to functional excitatory synapses. Nat Neurosci **15,** 477, 2012.
44. Mariani, J., Simonini, M. V., Palejev, D., Tomasini, L., Coppola, G., Szekely, A.M., Horvath, T.L., and Vaccarino, F.M. Modeling human cortical development in vitro using induced pluripotent stem cells. Proc Natl Acad Sci U S A **109,** 12770, 2012.
45. Muratore, C.R., Srikanth, P., Callahan, D.G., and Young-Pearse, T.L. Comparison and optimization of hiPSC forebrain cortical differentiation protocols. PLoS One **9,** e105807, 2014.
46. Kelava, I., and Lancaster, M.A. Stem cell models of human brain development. Cell Stem Cell **18,** 736, 2016.
47. Moya, N., Cutts, J., Gaasterland, T., Willert, K., and Brafman, D.A. Endogenous WNT signaling regulates hPSC-derived neural progenitor cell heterogeneity and specifies their regional identity. Stem Cell Reports **3,** 1015, 2014.
48. Wu, J., Rostami, M.R., Cadavid Olaya, D.P., and Tzanakakis, E.S. Oxygen transport and stem cell aggregation in stirred-suspension bioreactor cultures. PLoS One **9,** e102486, 2014.

49. McMurtrey, R.J. Analytic models of oxygen and nutrient diffusion, metabolism dynamics, and architecture optimization in three-dimensional tissue constructs with applications and insights in cerebral organoids. Tissue Eng Part C Methods **22,** 221, 2016.
50. Sen, A., Kallos, M.S., and Behie, L.A. Expansion of mammalian neural stem cells in bioreactors: effect of power input and medium viscosity. Brain Res Dev Brain Res **134,** 103, 2002.
51. Sargent, C.Y., Berguig, G.Y., Kinney, M.A., Hiatt, L.A., Carpenedo, R.L., Berson, R.E., and McDevitt, T.C. Hydrodynamic modulation of embryonic stem cell differentiation by rotary orbital suspension culture. Biotechnol Bioeng **105,** 611, 2010.
52. Ismadi, M.Z., Gupta, P., Fouras, A., Verma, P., Jadhav, S., Bellare, J., and Hourigan, K. Flow characterization of a spinner flask for induced pluripotent stem cell culture application. PLoS One **9,** e106493, 2014.
53. Imaizumi, K., Sone, T., Ibata, K., Fujimori, K., Yuzaki, M., Akamatsu, W., and Okano, H. Controlling the regional identity of hPSC-derived neurons to uncover neuronal subtype specificity of neurological disease phenotypes. Stem Cell Rep **5,** 1010, 2015.
54. Suzuki, I.K., and Vanderhaeghen, P. Is this a brain which I see before me? Modeling human neural development with pluripotent stem cells. Development **142,** 3138, 2015.
55. Swartz, M.A., and Fleury, M.E. Interstitial flow and its effects in soft tissues. Annu Rev Biomed Eng **9,** 229, 2007.
56. Hladky, S.B., and Barrand, M.A. Mechanisms of fluid movement into, through and out of the brain: evaluation of the evidence. Fluids Barriers CNS **11,** 26, 2014.
57. Kim, K.M., Choi, Y.J., Hwang, J.H., Kim, A.R., Cho, H.J., Hwang, E.S., Park, J.Y., Lee, S.H., and Hong, J.H. Shear stress induced by an interstitial level of slow flow increases the osteogenic differentiation of mesenchymal stem cells through TAZ activation. PLoS One **9,** e92427, 2014.
58. Bejoy, J., Song, L., and Li, Y. Wnt-YAP interactions in the neural fate of human pluripotent stem cells and the implications for neural organoid formation. Organogenesis **12,** 1, 2016.
59. Dupont, S., Morsut, L., Aragona, M., Enzo, E., Giulitti, S., Cordenonsi, M., Zanconato, F., Le Digabel, J., Forcato, M., Bicciato, S., Elvassore, N., and Piccolo, S. Role of YAP/TAZ in mechanotransduction. Nature **474,** 179, 2011.
60. Van Winkle, A.P., Gates, I.D., and Kallos, M.S. Mass transfer limitations in embryoid bodies during human embryonic stem cell differentiation. Cells Tissues Organs **196,** 34, 2012.
61. Tonti, G.A., Mannello, F., Cacci, E., and Biagioni, S. Neural stem cells at the crossroads: MMPs may tell the way. Int J Dev Biol **53,** 1, 2009.
62. Hahn-Dantona, E., Ramos-DeSimone, N., Sipley, J., Nagase, H., French, D.L., and Quigley, J.P. Activation of proMMP-9 by a plasmin/MMP-3 cascade in a tumor cell model. Regulation by tissue inhibitors of metalloproteinases. Ann N Y Acad Sci **878,** 372, 1999.
63. Van Hove, I., Verslegers, M., Buyens, T., Delorme, N., Lemmens, K., Stroobants, S., Gantois, I., D'Hooge, R., and Moons, L. An aberrant cerebellar development in mice lacking matrix metalloproteinase-3. Mol Neurobiol **45,** 17, 2012.
64. Luo, J. The role of matrix metalloproteinases in the morphogenesis of the cerebellar cortex. Cerebellum **4,** 239, 2005.
65. Fridley, K.M., Nair, R., and McDevitt, T.C. Differential expression of extracellular matrix and growth factors by embryoid bodies in hydrodynamic and static cultures. Tissue Eng Part C Methods **20,** 931, 2014.
66. Lau, L.W., Cua, R., Keough, M.B., Haylock-Jacobs, S., and Yong, V.W. Pathophysiology of the brain extracellular matrix: a new target for remyelination. Nat Rev Neurosci **14,** 722, 2013.
67. Tsien, R.Y. Very long-term memories may be stored in the pattern of holes in the perineuronal net. Proc Natl Acad Sci U S A **110,** 12456, 2013.

Address correspondence to:
Yan Li, PhD
Department of Chemical and Biomedical Engineering
FAMU-FSU College of Engineering
Florida State University
2525 Pottsdamer Street
Tallahassee, FL 32310

E-mail: yli@eng.fsu.edu

Received: October 1, 2016
Accepted: August 11, 2017
Online Publication Date: September 18, 2017